Testing the seesaw mechanisms via displaced right-handed neutrinos from a light scalar at the HL-LHC

Wei Liu,[1,*] Jiale Li,[2,†] Jing Li,[2,‡] and Hao Sun[2,§]

[1]*Department of Applied Physics, Nanjing University of Science and Technology, Nanjing 210094, People's Republic of China*

[2]*Institute of Theoretical Physics, School of Physics, Dalian University of Technology, No. 2 Linggong Road, Dalian, Liaoning 116024, People's Republic of China*

(Received 15 April 2022; accepted 8 July 2022; published 21 July 2022)

We investigate the pair production of right-handed neutrinos from the decay of a light $B-L$ scalar in the $U(1)_{B-L}$ model. The $B-L$ scalar mixes with the SM Higgs, and the physical scalar is required to be lighter than the observed Higgs. The produced right-handed neutrinos are predicted to be long-lived according to the type-I seesaw mechanism and yield potentially distinct signatures such as displaced-vertex and time-delayed leptons at CMS/ATLAS/LHCb, as well as signatures at the far detectors including CODEX-b, FACET, FASER, MoEDAL-MAPP, and MATHUSLA. We analyze the sensitivity reach at the High-Luminosity LHC for the right-handed neutrinos with masses of 2.5–30 GeV, showing that the active-sterile mixing with muons can be probed to $V_{\mu N} \sim 10^{-5}$ at CMS/ATLAS/LHCb using the displaced-vertex searches, and 1 order of magnitude lower at MATHUSLA/CMS using time-delayed lepton searches, reaching the parameter space of interest for type-I seesaw mechanisms.

DOI: 10.1103/PhysRevD.106.015019

I. INTRODUCTION

The existence of the tiny neutrino masses observed by neutrino oscillation experiments is one of the most mysterious problems in the Standard Model (SM). Type-I seesaw mechanisms can explain it by adding additional right-handed (RH) neutrinos to form both Dirac and Majorana mass terms, which in turn yield tiny active neutrino masses. Among the models that incorporate a type-I seesaw mechanism, an anomaly-free $U(1)_{B-L}$ model is considered as one of the simplest [1,2]. In this model, the RH neutrinos are charged under $B-L$ gauge, and therefore couple to the $B-L$ gauge boson Z'. It also contains an additional scalar χ which is responsible for introducing the Majorana masses of the neutrinos via the spontaneous symmetry breaking of $U(1)_{B-L}$. If the χ mixes with the SM Higgs, both the physical SM-like Higgs and the $B-L$ scalar s can couple to the RH neutrinos. Therefore, the RH neutrinos can be produced not only by the decay of the W/Z gauge bosons as in the minimal neutrino extension to the SM (νMSM) [3], but also via the decays of the SM Higgs, Z', and the scalar s.

RH neutrinos have been investigated at the LHC from the decays of W/Z gauge bosons, with limits of the active-sterile mixings set at $V_{lN} \lesssim 10^{-3}$ [4–15]. However, the type-I seesaw mechanisms indicate that $V_{lN} \approx \sqrt{\frac{m_\nu}{m_N}} \lesssim \sqrt{\frac{0.1\ \text{eV}}{\text{GeV}}} \approx 10^{-5}$ at the LHC. The searches for RH neutrinos via W/Z gauge boson decays can never reach such a parameter space, i.e., the production of RH neutrinos $\sigma \lesssim V_{lN}^2 \times \sigma(pp \to W \to l\nu) \lesssim 10^{-10} \times 10^7\ \text{fb} = 10^{-3}\ \text{fb}$, leading to no observation even in the high-luminosity era.

Meanwhile, the production of RH neutrinos via the scalar does not depend on the active-sterile mixings, and searches for this process at the LHC might lead to successful probes of type-I seesaw mechanisms. These RH neutrinos within such a parameter space can be regarded as long-lived particles (LLPs), as their decay length $L_N \approx 2.5\ \text{cm} \times (\frac{10^{-6}}{V_{lN}})^2 \times (\frac{100\ \text{GeV}}{m_N})^5$ [16,17] can potentially lead to vertices several meters away from the collision point. Once produced, they can yield distinct displaced vertex signatures at the LHC, which are almost background free. The final states of RH neutrinos can also be detected using the precision-timing information at CMS [18] and the upgrades of the ATLAS detectors. Aiming at probing such LLPs including RH neutrinos, several proposals for the construction of the far detectors at the lifetime

*wei.liu@njust.edu.cn
†lijiale@mail.dlut.edu.cn
‡lj948756370@mail.dlut.edu.cn
§haosun@dlut.edu.cn

frontier at the LHC have been put forward. Among them, the FASER [19] and MoEDAL-MAPP [20] detectors have been installed and will be in operation during Run 3 of the LHC. Other detectors—including CODEX-b [21], FACET [22], and MATHUSLA [23]—are still being discussed.

The $B-L$ scalar can be produced via gluon-gluon fusion at the LHC, by the mixings with the SM Higgs. Direct searches for additional Higgses and indirect searches via electroweak precision tests including the Higgs signal rates set limits on the mixings [24]. For a $B-L$ scalar heavier than the SM-like Higgs, the current limit for the mixings is $\sin\alpha \lesssim 0.3$. If the scalar is lighter than the SM-like Higgs, the limits are well constrained by the Higgs signal rates, $\sin\alpha \lesssim 0.06$. Given such low mixings, a light $B-L$ scalar can still be produced abundantly, reaching 10^3 fb [24,25]. Due to such low mixings with the SM sector, this light scalar has an appreciable decay branching ratio to RH neutrinos. Therefore, displaced RH neutrino production from the decay of a light $B-L$ scalar is a hopeful channel to search for RH neutrinos and test the seesaw mechanisms. Reference [26] looked at the possible scenario where the $B-L$ scalar is heavier than the SM-like Higgs. RH neutrinos decaying into a light s was also discussed in a recent paper [27].

Other than the $B-L$ scalar, the additional production of RH neutrinos in the $U(1)_{B-L}$ model has also been investigated in several papers. References [26,28–37] discussed RH production via the Z' boson, and mainly looked for their displaced final states at the lifetime frontiers. Some explorations at the FCC-hh for similar channels were studied in Refs. [38–40], and the production of RH neutrinos via the SM-like Higgs was studied in Refs. [17,41–49].

Since the production of RH neutrinos from light $B-L$ scalar decays is rarely studied, in this work we focus on the channel $pp \to s \to NN$. The light $B-L$ scalar has a mass within the range [10, 125] GeV, such that it is dominantly produced via gluon-gluon fusion at the LHC and is lighter than the observed Higgs. The light scalar subsequently decays to RH neutrinos, leading to distinct displaced-vertex and time-delayed leptons signatures. The cross section of this process depends on the Higgs mixing angle, the masses of the light scalar and RH neutrinos, as well as the Yukawa couplings of RH neutrinos. After summarizing the current limits, we choose a benchmark scenario from the allowed values and show that RH neutrinos from the decay of a light $B-L$ scalar still have an appreciable production cross section. We then estimate the sensitivity reach of this process using the displaced-vertex and time-delayed lepton searches at CMS/ATLAS and LHCb, as well as far detectors including CODEX-b, FACET, FASER, MoEDAL-MAPP, and MATHUSLA.

This paper is organized as follows. In Sec. II, we briefly review the $U(1)_{B-L}$ model, the decays of the light scalar s, and the current limits on the Higgs mixings as a function of the light scalar masses and the Yukawa couplings of RH neutrinos. The cross section of the pair production of RH neutrinos from the light scalar is given in Sec. III, followed by a summary of the displaced RH neutrinos analyses at the High-Luminosity LHC (HL-LHC) in Sec. IV. The estimated sensitivity is shown in Sec. V. Finally, we conclude in Sec. VI.

II. MODEL

In addition to the particle content of the SM, the scalar part of the $U(1)_{B-L}$ model consists of a SM singlet scalar field χ,

$$\mathcal{V}(H,\chi) = m^2\phi^\dagger\phi + \mu^2|\chi|^2 + \lambda_1(\phi^\dagger\phi)^2 + \lambda_2|\chi|^4 + \lambda_3\phi^\dagger\phi|\chi|^2. \tag{1}$$

After diagonalization of the mass matrix, the additional scalar singlet χ mixes with the SM Higgs [24],

$$\begin{pmatrix} h \\ s \end{pmatrix} = \begin{pmatrix} \cos\alpha & -\sin\alpha \\ \sin\alpha & \cos\alpha \end{pmatrix} \begin{pmatrix} \phi \\ \chi \end{pmatrix}, \tag{2}$$

where α is the mixing angle between the scalar fields, and h and s are the SM-like Higgs and $B-L$ scalar mass eigenstates, respectively. We take 10 GeV $< m_s < m_h =$ 125 GeV. Therefore, the s is dominantly produced via s-channel gluon-gluon fusion, and $\sigma(pp\to s) \approx \sin\alpha^2 \times \sigma(pp\to s,\mathrm{SM})$, whereas $\sigma(pp \to s, \mathrm{SM})$ is the cross section when s has the same couplings as the SM Higgs, which can be inferred from Ref. [25]. The current limits of $\sin\alpha$ for such m_s is shown in the left panel of Fig. 1 [24,50], which was obtained from Ref. [24] using LHC Run 1 results. They are set mainly by the measurements of the Higgs signal rates [24] and are still valid, as shown in Ref. [50] using Run 2 results. So $\sin\alpha \lesssim 0.06$ is allowed for such a scalar, and we take $\sin\alpha$ at the upper limits as our benchmark. A lighter s is also possible. For $m_s \sim \mathcal{O}$ GeV, the Higgs mixings are well constrained by the searches for rare meson decays; see Ref. [51] for details. $B^+ \to K^+ + \mathrm{inv}$ sets $\sin\theta \lesssim 10^{-3}$ for $m_s < 2$ GeV, and $K^+ \to \pi^+ + \mathrm{inv}$ sets $\sin\theta \lesssim 10^{-4}$ for $m_s < 0.36$ GeV [52,53]. For an even lighter scalar, the observation of the neutron star merges can be used to set limits, as shown in Ref. [54].

The fermion part of the Lagrangian includes additional neutrino mass terms,

$$\mathcal{L} \supset y_N\chi\bar{N}^cN + y_D\bar{L}\Phi N + \mathrm{H.c.}, \tag{3}$$

where we have omitted the difference between the weak and physical RH neutrinos.

Therefore, the $B-L$ scalar s can decay into pairs of RH neutrinos, and the partial width is expressed as

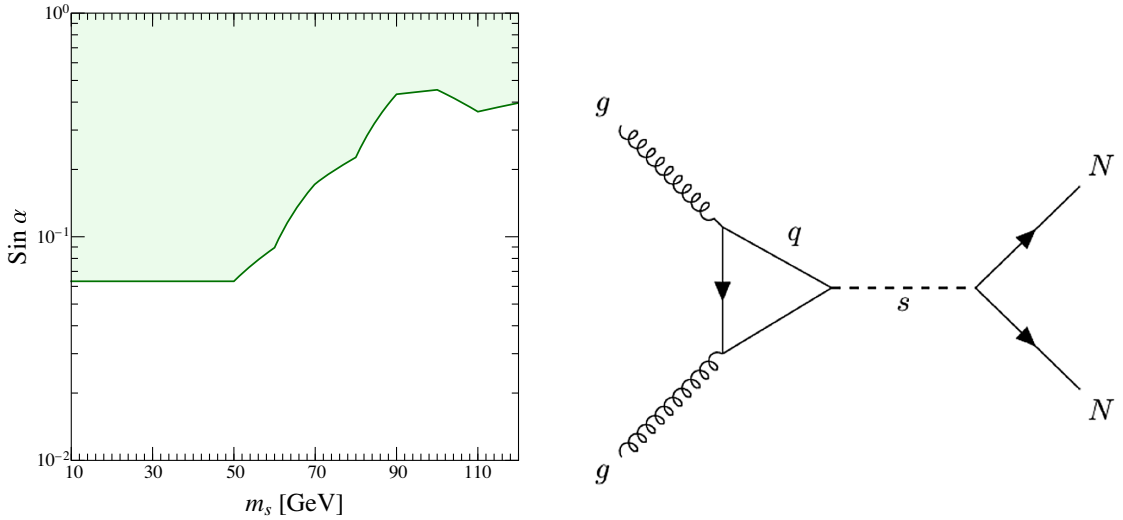

FIG. 1. Left: current limits at $(m_s, \sin\alpha)$ for 10 GeV $< m_s \leq m_h$ [24,55,56], where the green shaded region is ruled out by experiments. Right: Feynman diagrams of the main process $pp \to s \to NN$.

$$\Gamma_{s\to NN} = \frac{1}{2}\cos^2\alpha \cdot \frac{y_N^2 m_s}{8\pi}\left(1-\frac{4m_N^2}{m_s^2}\right)^{3/2} \approx \frac{1}{2}\cdot\frac{y_N^2 m_s}{8\pi}\left(1-\frac{4m_N^2}{m_s^2}\right)^{3/2}, \quad (4)$$

where $y_N = \frac{\sqrt{2}m_N}{2v_s}$ and $v_s \gtrsim 3.5$ TeV for $m_{Z'} \gtrsim 1$ TeV from electroweak precision observable (EWPO) [57,58]. Although CMS/ATLAS dijet searches yield better limits as $v_s \gtrsim 25$ TeV for $m_{Z'} \leq 5$ TeV [59], we can still take $v_s = 10$ TeV as our benchmark assuming the gauge boson Z' is very heavy beyond the reach of current direct searches, and therefore only the indirect limits from EWPO apply.

The branching ratio for $s \to NN$ is

$$\mathrm{BR}_{s\to NN} = \frac{\Gamma_{s\to NN}}{\sin^2\alpha\Gamma_{s,SM} + \Gamma_{s\to NN}}. \quad (5)$$

Since the mixing $\sin\alpha$ is tiny, the only appreciable decay width comes from $s \to b\bar{b}, c\bar{c}, \tau\bar{\tau}$ and $s \to NN$.

The RH neutrinos N mix with the active neutrinos via the active-sterile mixings V_{lN}. The decay length of N is a function of m_N and V_{lN}, such that [16,17]

$$L_N \approx 2.5\ \mathrm{cm} \times \left(\frac{10^{-6}}{V_{lN}}\right)^2 \times \left(\frac{100\ \mathrm{GeV}}{m_N}\right)^5. \quad (6)$$

As the type-I seesaw mechanisms predict $V_{lN} \lesssim 10^{-5}$, the N can be long lived with meters of decay length. We focus on the RH neutrinos which only mix with the muon, and hence $V_{lN} \equiv V_{\mu N}$, so the final states of N can be looked for via the searches for displaced vertices at the muon chamber.

Before we proceed with detailed calculations, we summarize the benchmark parameters in Table I. They are chosen to optimize the discovery potential from the allowed values in current limits.

TABLE I. Benchmark parameters in this paper.

Parameters	$\sin\alpha$	m_s	m_N	v_s
Values	0.06	10–125 GeV	$m_s/4$	10 TeV

III. PRODUCTION CROSS SECTION

In order to estimate the production cross section of the $pp \to s \to NN$ process, we can apply the narrow width approximation,

$$\sigma(pp \to s \to NN) = \sin\alpha^2 \times \sigma(pp \to s, \mathrm{SM}) \times \mathrm{BR}_{s\to NN}. \quad (7)$$

The production of the s via gluon-gluon fusion at N^{3}LO is shown in the left panel of Fig. 2, which is taken from Ref. [25] and scaled to the 14 TeV LHC [60]. The N^{3}LO effects of gluon-gluon fusion can enhance the production of the s by a factor of $\mathcal{O}(10^2)$. The right panel of Fig. 2 illustrates the branching ratio $\mathrm{BR}_{s\to NN}$ as a function of m_s. As m_N becomes larger, the Yukawa coupling y_N increases, resulting in a larger partial width and branching ratio, reaching 25% when $m_N \approx 100$ GeV. Nevertheless, there is a bump near where $m_s \approx 2m_b$. The increased m_s leads to a larger phase space for the $s \to b\bar{b}$ channel and a smaller $\mathrm{BR}_{s\to NN}$.

To analyze the kinematical distribution and later the sensitivity, we perform a Monte Carlo simulation with the following steps. First, we use the universal FeynRules output format (UFO) [61] of the $B-L$ model developed in Ref. [17], which is also publicly available from the FeynRules [62,63] model database [64]. Then, it is fed

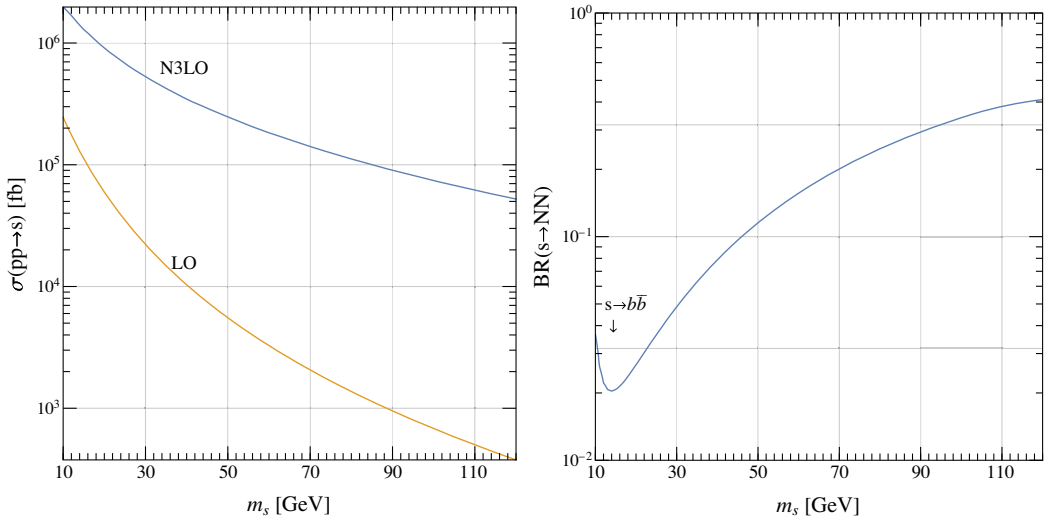

FIG. 2. Left: $\sigma(pp \to s)$ as a function of m_s at the 14 TeV LHC, for SM-like couplings. Right: BR$(s \to NN)$ as a function of m_s. We fix $m_N = \frac{m_s}{4}$ and $v_s = 10$ TeV.

into the Monte Carlo event generator MadGraph5aMC@NLO v2.6.7 [65] for parton-level simulation. Afterwards, the initial- and final-state parton shower, hadronization, heavy hadron decays, etc. are taken care by PYTHIA v8.235 [66]. The clustering of the events is performed by FastJet v3.2.1 [67]. Detector effects are not taken into account at this stage, while some simplified cuts are taken in the next section to roughly describe the detector effects in detecting LLPs. Finally, we use inverse sampling to generate the exponential decay distribution of RH neutrinos.

After the simulation, we show the cross section $pp \to s \to NN$ for fixed sin $\alpha = 0.06$ and running sin α in the left and right panels of Fig. 3, respectively. Although the production cross section $\sigma(pp \to s)$ drops for heavier s, it is compensated by the growing branching ratio, resulting in an almost constant $\sigma(pp \to s \to NN) \approx 70$ fb for $m_s \gtrsim 20$ GeV. The proposed Higgs factories—such as the ILC, CEPC, and FCC-ee—will have the potential to determine the Higgs couplings by an order of magnitude or even higher [68], leading to stringent limits on the Higgs mixings $\sin\alpha \lesssim 0.01$ [69]. Nevertheless, potential observation is still available even for $\sin\alpha \sim 10^{-3}$.

Therefore, the pair production of RH neutrinos from a light $B - L$ scalar has a sufficient cross section at the LHC. Given the high luminosity and the potential far detectors optimized for LLP detection, the HL-LHC is hopeful to probe RH neutrinos. In the following section, we demonstrate dedicated analyses for the distinct displaced-vertex signature of RH neutrinos according to different detectors at the HL-LHC.

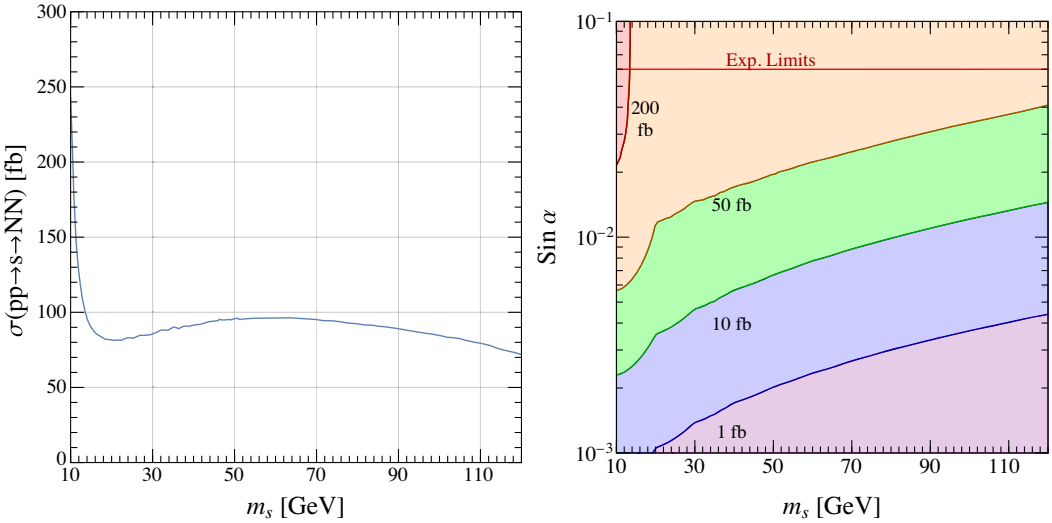

FIG. 3. $\sigma(pp \to s \to NN)$ as a function of m_s for sin $\alpha = 0.06$ (left) and as a function of m_s and sin α (right) at the LHC. We fix $m_N = \frac{m_s}{4}$.

IV. ANALYSES OF THE DISPLACED RH NEUTRINOS

We outline the relevant properties of the detectors to the efficiencies of LLP detection. These include their locations to the interaction points (IP) where the protons collide, the geometrical sizes, the trigger requirements and the reconstruction efficiencies. Considering all of these effects, the expected number of observed events can be expressed as

$$N_{\rm signal}/\mathcal{L} = \sigma(pp \to s \to NN) \times {\rm BR}(N \to \text{final states}) \times \epsilon_{\rm kin} \times \epsilon_{\rm geo} \times \epsilon_{\rm recon}, \quad (8)$$

where $\mathcal{L}$ is the integrated luminosity, and $\epsilon_{\rm kin}$ and $\epsilon_{\rm geo}$ are the efficiencies due to the trigger requirements and geometrical acceptance, respectively. $\epsilon_{\rm recon}$ is the reconstruction efficiencies, which we assume to be 100% for all detectors except the LHCb. As N dominantly decays to μjj, we focus on these final states and consider at least one muon and one jet with $\Delta R(\mu j) > 0.3$ to form a displaced vertex. When look for RH neutrinos, we only consider one N to decay into μjj and displaced, while no consideration is required on the other N decays, while we do not put any requirements on the other N decays, i.e., they can decay into any possible products.

a. CMS and ATLAS are two general detectors in the transverse direction of the LHC. Although they are designed to detect prompt decay products, there are several existing search strategies to look for LLPs from the displaced muon-jet (DMJ) and time-delayed (Timing) signals.

The displaced muon-jet search was proposed in Ref. [70]. The original analysis was optimized for inelastic dark matter, as it has similar signatures to RH neutrinos; we employ the same strategy:

$$\begin{aligned} \text{DMJ:}\ & p_T(j) > 120\ \text{GeV}, \\ & p_T(\mu) > 5\ \text{GeV}, \\ & L_{xy}(N) < 0.3\ \text{m}, \\ & |\eta(N)| < 2.5, \\ & d_\mu > 1\ \text{mm}. \end{aligned} \quad (9)$$

The N is required to decay inside the outer layer of the tracking system to give precise tracks, so its transverse decay length satisfies $L_{xy}(N) < 0.3$ m. A vertex is considered to be sufficiently displaced if the transverse distance between the momentum of the muon and that of the N is significant, i.e., d_μ is larger than the resolution of the detector.

Reference [18] proposed an alternative analysis using the precision-timing information of the CMS detector. The decays of RH neutrinos lead to a secondary vertex, so the muon in the final state when reaching the timing layer will be delayed due to the decreased speed of the N and larger path length compared to the SM particles traveling in a straight line. The cuts for the time-delayed signatures are

$$\begin{aligned} \text{Timing:}\ & p_T(j) > 120(30)\ \text{GeV}, \\ & p_T(\mu) > 3\ \text{GeV}, \\ & \Delta t > 0.3\ \text{ns}, \\ & 0.05\ \text{m} < L_{xy}(N) < 1.17\ \text{m}, \\ & L_z(N) < 3.04\ \text{m}. \end{aligned} \quad (10)$$

The $p_T(j)$ cuts are applied on a jet from initial-state radiation, which is identified following Ref. [71] to time stamp the primary vertex. The calculation of the time delay Δt is described in the Appendix. The event with a lepton that has a time delay larger than the resolution of the CMS timing detector is regraded as a signal. The RH neutrinos are required to decay within the timing layer. The trigger for the jets is required to be lowered to $p_T(j) > 30$ GeV as an optimized case [72].

b. LHCb is a general detector optimized for B physics in the forward direction of the LHC. A dedicated search employed by the LHCb experiment [73] can be used to identify the displaced signatures of RH neutrinos, as described in Ref. [74]. The search strategy is

$$\begin{aligned} \text{LHCb:}\ & N(j) > 0, && p_T(j) > 20\ \text{GeV}, && \\ & N(\mu) = 1, && p_T(\mu) > 12\ \text{GeV}, && \\ & && 2 < |\eta(j,\mu)| < 5, && \\ & && m_N > 4.5\ \text{GeV}, && \\ & 0.005\ \text{m} < L_{xy}(N) < 0.02\ \text{m}, && L_z(N) < 0.4\ \text{m}, && \epsilon_{\rm recon} = 50\%, \\ & 0.02\ \text{m} < L_{xy}(N) < 0.5\ \text{m}, && L_z(N) < 0.4\ \text{m}, && \epsilon_{\rm recon} = 100\%, \\ & 0.005\ \text{m} < L_{xy}(N) < 0.6\ \text{m}, && 0.4\ \text{m} < L_z(N) < 2\ \text{m}, && \epsilon_{\rm recon} = 50\%. \end{aligned} \quad (11)$$

In the original literature there were no p_T cuts for the jets; nevertheless, we add a soft cut to roughly consider the general LHCb trigger requirements. The first and third regions mentioned are parts of the trigger tracker tracking station. The reconstruction efficiencies are reduced due to backgrounds and blind spots related to the detector. The second region is the vertex locator, in which the reconstruction efficiencies for the displaced vertex should be high.

c. FASER: Despite the existing general-purpose detectors, specialized detectors with macroscopic distance from the IP are optimized for LLP discovery. If LLPs are light and weakly coupled, they should possess low transverse momentum and travel in a very forward direction, collimated with the beam axis, and therefore they cannot be detected by the general LHC detectors. Aiming at probing these particles, the Forward Search Experiment (FASER) detector has been proposed and installed [19,75]. It should start to collect data during Run 3 of the LHC. It is placed 480 meters away from the ATLAS IP, in the side tunnel TI18. In order to detect LLPs including RH neutrinos, FASER requires them to decay inside the detector volume,

$$\begin{aligned}\text{FASER}:\ & L_{xy} < 1\ \text{m},\\ & 475\ \text{m} < L_z < 480\ \text{m},\\ & E_{vis} > 100\ \text{GeV}.\end{aligned} \tag{12}$$

The above design is actually phase 2 of the FASER at the HL-LHC. A smaller detector volume is employed for the phase 1 design. Here we only consider phase 2 to maximize the detection probability. The requirement for the total energy of the visible particles is to reduce the trigger rate of low energy that might come from the background.

d. The Monopole Apparatus for Penetrating Particles (MoEDAL-MAPP) is a proposed subdetector of the MoEDAL detector [20]. The original MoEDAL detector is a specialized detector at the LHCb IP that is designed to look for magnetic monopoles and is not able to detect the decays of new particles. The MAPP subdetector was proposed to solve this problem especially for detecting LLPs. Like FASER, it has already been installed and should begin taking data during Run 3 of the LHC. Its search strategy for RH neutrinos is

$$\begin{aligned}\text{MoEDAL-MAPP}:\ & 3\ \text{m} < L_x < 6\ \text{m},\\ & -2\ \text{m} < L_y < 1\ \text{m},\\ & 48\ \text{m} < L_z < 61\ \text{m},\\ & E_{track} > 0.6\ \text{GeV}.\end{aligned} \tag{13}$$

The original MoEDAL-MAPP detector actually has a ring-like shape; here, we roughly consider it as a cuboid to simplify the calculation. The threshold on the track energies is applied to roughly describe the trigger requirements, which were originally introduced in Ref. [21] for the CODEX-b experiment. Nevertheless, we introduce such trigger cuts for all of the following far detectors as a baseline.

e. The Compact Detector for Exotics at LHCb (CODEX-b) is a proposed detector located in the LHCb cavern, which is unoccupied after the Run 3 upgrade of the LHCb [21]. It can be used to detect RH neutrinos by requiring

$$\begin{aligned}\text{CODEX-b}:\ & 26\ \text{m} < L_x < 36\ \text{m},\\ & -3\ \text{m} < L_y < 7\ \text{m},\\ & 5\ \text{m} < L_z < 15\ \text{m},\\ & E_{track} > 0.6\ \text{GeV}.\end{aligned} \tag{14}$$

f. The Forward-Aperture CMS Extension (FACET) is a newly proposed long-lived particle detector in the very forward region of the CMS experiment [22]. It is designed to be a new subsystem of CMS, as it uses the same technology and is fully integrated. Therefore, the CMS main detector and its correlation can be studied, which is interesting for the SM physics programs in low pileup collisions. Therefore, studies of the correlations between the main detector of CMS and it can be made available, which is interesting for the SM physics programs in low pileup collisions. Its search strategy for RH neutrinos is

$$\begin{aligned}\text{FACET}:\ & 0.18\ \text{m} < L_{xy} < 0.5\ \text{m},\\ & 101\ \text{m} < L_z < 119\ \text{m},\\ & E_{track} > 0.6\ \text{GeV}.\end{aligned} \tag{15}$$

g. The Massive Timing Hodoscope for Ultra-Stable Neutral Particles (MATHUSLA) is the largest proposed detector aimed for LLPs [23]. It is placed on the surface of ATLAS or CMS. We employ the following cuts to probe RH neutrinos using MATHUSLA:

$$\begin{aligned}\text{MATHUSLA}:\ & 100\ \text{m} < L_{xy} < 120\ \text{m},\\ & -100\ \text{m} < L_y < 100\ \text{m},\\ & 100\ \text{m} < L_z < 300\ \text{m},\\ & E_{track} > 0.6\ \text{GeV}.\end{aligned} \tag{16}$$

Given the search strategy of all of the detectors at the lifetime frontiers, a comparison between them can be useful. The most important parameter of these detectors is their geometrical reach both in the angle and the distance. Therefore, we give the comparison of these detectors in the left panel of Fig. 4 for their reach in distance to the corresponding IP, and in the right panel of Fig. 4 for their reach in angle to the beam axis. The distribution of the (p_N, θ) information of the decayed RH neutrinos is also shown in the right panel of Fig. 4 for comparison, which is obtained from a benchmark where $m_N = 10$ GeV and

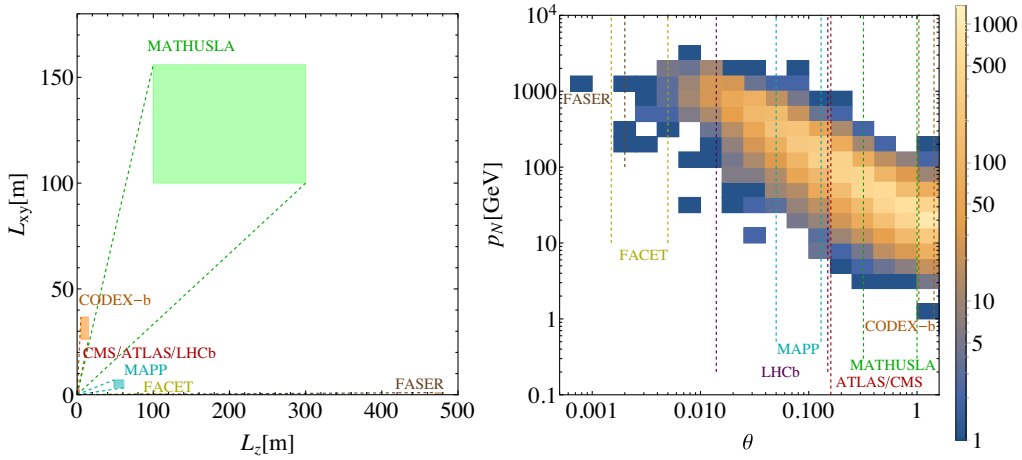

FIG. 4. The reach of the detectors in the distance to the IP, at (L_{xy}, L_Z) plane (left) and (p_N, θ) (right) plane. The (p_N, θ) information of the decayed RH neutrinos is also shown in the right panel for comparison, obtained from a benchmark where $m_N = 10$ GeV and $m_s = 40$ GeV. The number of right-handed neutrinos from 10^4 events is represented by the colors as indicated by the legend band.

$m_s = 40$ GeV. This helps to estimate the kinematical and geometrical efficiencies of each detector. The (p_N, θ) of RH neutrinos are roughly distribute around the line where $p_N \times \theta \equiv p_T(N) \approx 10$ GeV, which is the expectation value of the $p_T(N)$ for each RH neutrino from a s with 40 GeV mass decaying to two N with 10 GeV. From the figures, the combined reach of all of these detectors roughly covers the full range of θ, except for a small region where $\theta \sim 10^{-2}$, advocating a potential new detector to be placed to probe new particles with certain masses. It is clear that FASER and FACET are placed in a very forward direction, where RH neutrinos are rarely distributed at this benchmark, which might lead to negligible sensitivity. Other detectors are able to probe RH neutrinos at different angles and distances. Among them, LHCb and MAPP are in the forward direction, while MAPP covers smaller region in angle, inside the LHCb coverage. Nevertheless, MAPP is located much further than the LHCb, capable to probe RH neutrinos with larger decay length. MATHUSLA, ATLAS/CMS, and CODEX-b are placed in the transverse direction. Although MATHUSLA is enormous in size, due to its large distance to the IP, its angular coverage is inside CMS/ATLAS. CODEX-b lacks in angular size, only covers a small region in the very transverse direction.

CMS/ATLAS and LHCb analyses employ hard trigger cuts on the transverse momentum of the jets. To estimate the kinematical efficiencies ϵ_{kin} due to these cuts, we illustrate the $p_T(j)$ (left) and η_j (right) of the final-state jets from N decays in Fig. 5, taking from the benchmark where $m_N = 10$ GeV and $m_s = 40$ GeV. The lower threshold on $p_T(j)$ is due to the FastJet algorithm. Only 0.1% of events survive after the $p_T(j) > 120$ GeV cut. While $\mathcal{O}(100)$ times more events can left if the cut is lowered to $p_T(j) > 30$ GeV. Hence, the relaxed $p_T(j)$ requirement

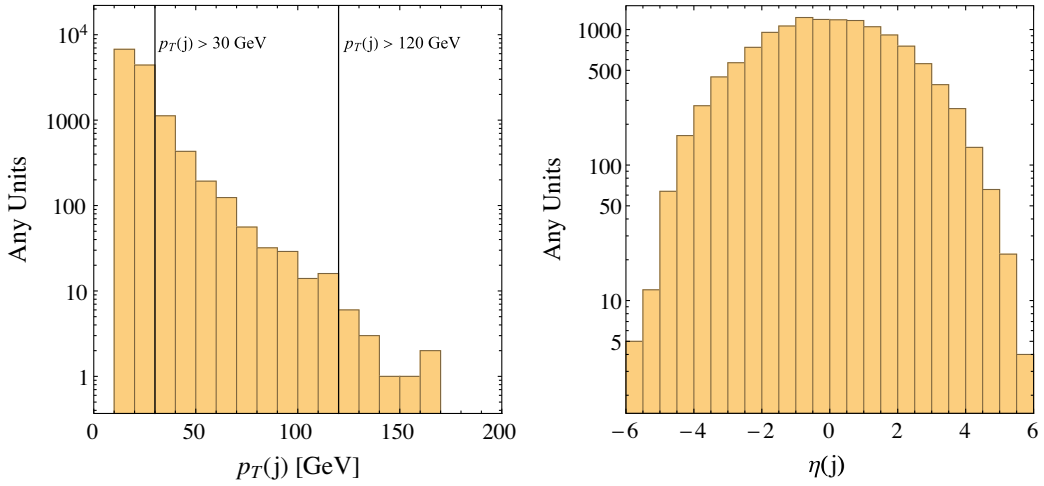

FIG. 5. Kinematical distributions of $p_T(j)$ (left) and η_j (right) of the final-state jets from N decays. We take $m_N = 10$ GeV and $m_s = 40$ GeV.

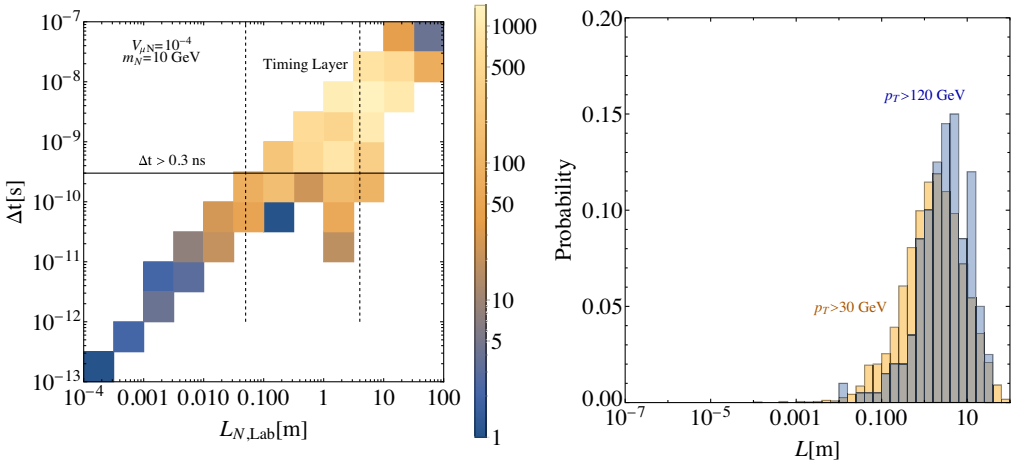

FIG. 6. Left: time-delay Δt distribution and the distribution of the corresponding laboratory decay length of RH neutrinos $L_{N,\mathrm{Lab}}$ with $p_T(j) > 120$ GeV cuts. The number of right-handed neutrinos from 10^4 events is represented by color, as indicated in the legend. The signal event is required to have a time-delay that is sufficiently larger than the resolution of the detector, i.e., $\triangle t > 0.3$ ns [18]. Right: $L_{N,\mathrm{Lab}}$ distribution for two time-delayed analyze with $p_T(j) > 120(30)$ GeV. The distribution is obtained from a benchmark where $m_N = 10$ GeV, $m_s = 40$ GeV and $V_{\mu N} = 10^{-4}$.

compared to the DMJ analysis is favorable to increase the detection ability. In the right panel of Fig. 5 we show that jets like N are likely to be discovered in the transverse direction.

The time-delayed analyze is unique, so we need special information to estimate its kinematical and geometrical efficiencies. In the left panel of Fig. 6 we show the distribution of the time delay Δt and the corresponding laboratory decay length of RH neutrinos $L_{N,\mathrm{Lab}}$, which is obtained from a benchmark where $m_N = 10$ GeV, $m_s = 40$ GeV, and $V_{\mu N} = 10^{-4}$ with $p_T(j) > 120$ GeV cuts. The solid horizontal line indicates the cut $\Delta t > 0.3$ ns, and the vertical lines show the region inside the timing layer. Most of the points are distributed around the line where $L_{N,\mathrm{Lab}} \sim c\Delta t$, as RH neutrinos are boosted traveling in speed closing to the speed of the light c, this means $l_l \sim l_{\mathrm{SM}}$ so the l and N travel in similar directions; see the Appendix. At this benchmark, the time-delayed analyses capture most of the signal events, as vastly events are within the region where they possess sufficient time delay and RH neutrinos are decay within the timing layer. Things become different if the benchmark is changed, as the distribution will be modified according to its expected proper decay length and the Lorentz factor. Nevertheless, the distribution should still follow the $L_{N,\mathrm{Lab}} \sim c\Delta t$ line, and the different benchmark just changes the peak where most of the points are distributed. We can expect that with a lower $V_{\mu N}$ or m_N, the expected lab decay length would be larger, and therefore the events are likely to move to the upper right corner, and vice versa. As the threshold of the time delay depends on the resolution of the timing detector, which can be improved with more advanced techniques, it becomes interesting to see how the improved resolution can help to detect more signal events. However, as illustrated in the figure, since $L_{N,\mathrm{Lab}} \sim c\Delta t$, as $c\Delta t_{\mathrm{min}} \approx L_{xy,\mathrm{min}} = 0.05$ m of the timing layer, only improving Δt distribution will not help to increase the efficiencies. One needs to put the timing layer closer to the IP at the same time, or extend the timing layer to the muon system to make the time-delayed analyses more efficient. We have provided two time-delayed analyses with different $p_T(j)$ thresholds, as more energetic jets are likely to come from more boosted RH neutrinos with larger Lorentz factors, the distribution of the $L_{N,\mathrm{Lab}}$ changes as shown in the right panel of Fig. 6. Lowering the $p_T(j)$ threshold introduces additional effects such that the lab decay length of RH neutrinos is likely to become smaller. This makes the two analyses sensitive to RH neutrinos with different proper decay lengths, and the corresponding parameter space $(m_N, V_{\mu N})$, which we show in the following section.

V. SENSITIVITIES

With all of the analysis methods and the estimation of the efficiencies in hand, we calculate the sensitivity of the above detectors. LHCb, MoEDAL-MAPP, and CODEX-b have an integrated luminosity of 300 fb^{-1} at the HL-LHC, whereas the rest of the detectors have 3000 fb^{-1}. As most of the analyses in the original references considered a negligible background, since the decays of the LLPs are rare in the SM, we make this optimistic assumption as well when estimating the sensitivity. Therefore, the sensitivity is obtained via requiring $N_{\mathrm{signal}} > 3.09$ from the Poisson distribution at 95% C.L.

The resulting sensitivity at 95% C. L. in the $(m_N, V_{\mu N})$ plane of the seesaw parameters for all of the detectors is shown in Fig. 7. The grey shaded region labeled "Current" is the current best limits from the existing searches for RH

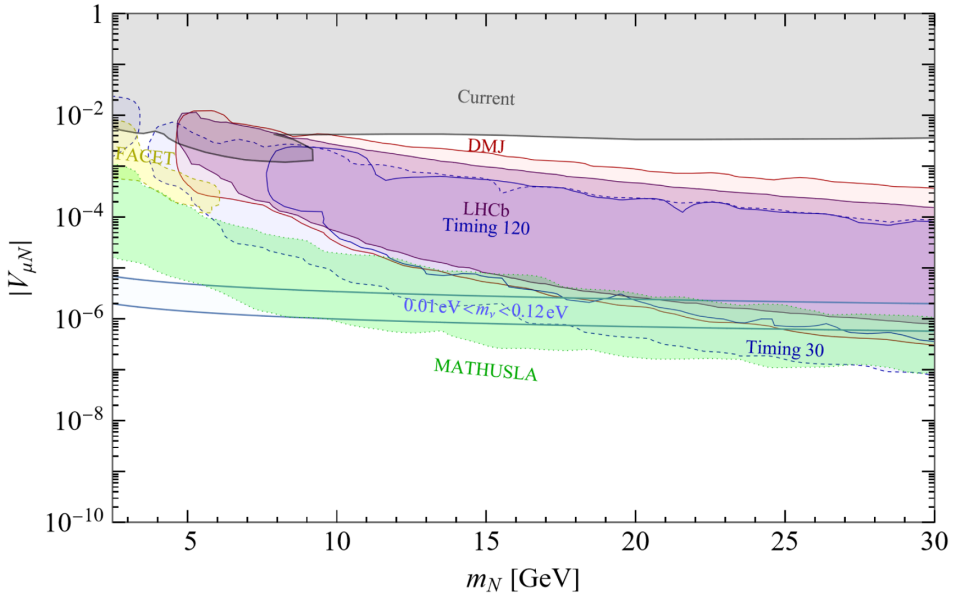

FIG. 7. Sensitivity of the DMJ and time-delayed analyses with $p_T(j) > 120$ GeV (Timing 120) and $p_T(j) > 30$ GeV (Timing 30) at the CMS/ATLAS detectors and LLP searches at the CODEX-b, FACET and MATHUSLA detectors at the HL-LHC to the $(m_N, V_{\mu N})$ plane. The FASER and MoEDAL-MAPP detectors have negligible sensitivity. The grey shaded region labeled "Current" is the current best limits from the existing searches for RH neutrinos [76]. The light blue band corresponds to the regime with light neutrino masses $0.01\ \text{eV} < m_\nu < 0.12\ \text{eV}$ via the type-I seesaw mechanism [77,78].

neutrinos [76]. The existing searches are performed via only searching for the processes involving RH neutrinos within the νMSM, such as the $pp \to W \to Nl$ processes, since there exists at least one light neutrino with a mass within the range $0.01\ \text{eV} < m_\nu < 0.12\ \text{eV}$ from neutrino oscillation experiments and cosmological observations [77,78]. We indicate the parameter space predicted by the type-I seesaw mechanism, i.e., $V_{lN} \approx \sqrt{m_\nu/m_N}$, as the light blue shaded band ("seesaw band"). To test the type-I seesaw mechanism, the sensitivity reach of the detectors needs to cover the seesaw band. From Fig. 7, all of the sensitivity reach of the detectors for displaced RH neutrinos covers the region from left top to right bottom corner, basically follows the curves of certain proper decay length of the N.

When performing the DMJ and Timing analyses, the CMS/ATLAS detectors can be sensitive to a large parameter space extending from $V_{\mu N} \sim 10^{-2}$ to 10^{-5}, roughly filling the region between the current best limits and the seesaw band. They can only probe a part of the seesaw region when $m_N \gtrsim 25$ GeV. The DMJ analysis has a threshold on the m_N, which is due to the $p_T(j) > 120$ GeV cut. The sensitivity should recover for very light N, near $m_N \sim 3$ GeV. The sensitivity covers a larger range in $V_{\mu N}$ for heavier N, since the penalty in the production cross section is not competitive with the gain in kinematical efficiencies. The Timing analysis with the $p_T(j) > 120$ GeV threshold (Timing 120) is sensitive to a similar parameter space, and only lacks reach for larger $V_{\mu N}$ compared to the DMJ analysis due to the $L_{xy} > 0.05$ m requirement from the timing layer. Lowering the $p_T(j)$ threshold to 30 GeV (Timing 30) helps to reach a much larger parameter space, for both lighter N and lower $V_{\mu N}$. The latter is due to the larger cross section. However, this should allow us to reach larger $V_{\mu N}$ as well. But, as shown in the right panel of Fig. 6, the $p_T(j) > 30$ GeV cut selects more RH neutrinos with lower Lorentz factors and therefore shorter lab decay lengths. The gain in cross section is canceled by the lower geometrical efficiencies, as the lab decay length of RH neutrinos becomes too short to be captured by the timing layer at the upper edge of the reach in $V_{\mu N}$. As for testing the seesaw mechanism, the Timing 30 analysis can fully cover the seesaw band for $m_N \gtrsim 10$ GeV.

The displaced-vertex search at the LHCb roughly reach the similar region to the DMJ analysis of CMS/ATLAS, except the upper edge in $V_{\mu N}$ due to the $L_{xy} > 0.005$ m requirement. The LHCb analysis can capture softer RH neutrinos, enlarging the kinematical efficiencies; however, this is canceled by the 10 times smaller integrated luminosity of the LHCb IP.

The proposed far detectors are expected to be more sensitive to long-lived RH neutrinos, and probe smaller $V_{\mu N}$. Nonetheless, FASER and MoEDAL-MAPP (which are still being installed) as well as CODEX-b have shown negligible sensitivity in the whole parameter space. As described in the right panel of Fig. 4, FASER is placed too far forward, such that the RH neutrinos we considered are not captured. Since a RH neutrino mass $m_N = m_s/4 > 2.5$ GeV is chosen, RH neutrinos can travel in more

forward directions if the s or N is lighter. Such ab s should be produced by rare meson decays, and we leave this topic for future works. MoEDAL-MAPP and CODEX-b fail to probe any parameter space because of the low luminosity of the LHCb IP and its small angle coverage, as shown in the right panel of Fig. 4.

The FACET detector, placed at a very forward direction of CMS, can probe light RH neutrinos with $m_N \lesssim 5$ GeV. However, its reach is already covered by the Timing 30 analysis and is far away from the seesaw band. Moving to the MATHUSLA detector, due to its large length to the IP, it is sensitive to very long-lived N and therefore small mixings $V_{\mu N}$, covering the seesaw band from 5 GeV $\lesssim m_N \lesssim 25$ GeV. The lower end of the sensitivity of MATHUSLA can reach $V_{\mu N} \sim 10^{-7}$, exceeding other detectors by at least 1 order of magnitude, except for the Timing 30 analysis, as it has yield similar reach.

VI. CONCLUSION

The discovery of tiny neutrino masses indicates strong evidence for physics beyond the SM. The type-I seesaw mechanism is one of the most elegant ways to explain such neutrino masses by adding RH neutrinos. With the leptogenesis mechanism, RH neutrinos can also serve as the source of the baryon asymmetry of the Universe. Therefore, they have become one of the most attractive particles to look for in experiments.

Nevertheless, the searches for RH neutrinos at the LHC cannot explore the seesaw mechanism, due to the suppressed production of RH neutrinos from the SM W/Z boson decays. While the original type-I seesaw mechanism does not explain the origin of the Majorana masses, they can be generated by the spontaneous symmetry breaking of the $B-L$ symmetry. This introduces an additional production of RH neutrinos via the decay of the $B-L$ scalar. Such channel is rarely investigated while still experimentally allowed, so we focused on this channel and considered the muon flavor of RH neutrinos.

The type-I seesaw mechanism predicts long-lived RH neutrinos, which lead to a displaced-vertex signature. Aiming at this distinct signature, we considered searches for displaced RH neutrinos at the HL-LHC by using displaced muon jets, the time-delayed analyses at CMS/ATLAS, and the displaced-vertex analyses at the LHCb, FASER, MOEDAL-MAPP, CODEX-b, FACET, and MATHUSLA detectors.

We determined the sensitivity of the HL-LHC of the above detectors for the channel $pp \to s \to NN$. The scalar s is chosen to be lighter than the observed Higgs, 10 GeV $< m_s <$ 125 GeV, and it is produced via mixing with the SM Higgs, with the mixing angle fixed at $\sin\alpha = 0.06$. Measurements of the Higgs properties at the proposed Higgs factories might lead to more stringent limits on the Higgs mixing angle, such as $\sin\alpha \lesssim 0.01$. Nevertheless, we can still expect a positive sensitivity, as the cross section is expected to decrease by only 10 times at most, as shown in the right panel of Fig. 2, since the branching ratio of $s \to NN$ becomes larger for smaller mixings. A lighter s is also possible, mainly through meson decays, which we leave to future work.

Among the detectors, FASER, MoEDAL-MAPP, and CODEX-b do not show any sensitivity to the regions of interest where 2.5 GeV $< m_N <$ 30 GeV, while FACET can only probe the small region $m_N \lesssim 5$ GeV. CMS and LHCb are sensitive to $m_N \gtrsim 5$ GeV, which roughly fills the region between the current best limits and the seesaw region. Without equipping far detectors, lowering the p_T threshold of the timing analysis can already help CMS/ATLAS to test the seesaw mechanism for $m_N \gtrsim 10$ GeV, and achieve the active-sterile mixings as low as $V_{\mu N} \sim 10^{-7}$, which is comparable to MATHUSLA. However, MATHUSLA can still show better sensitivity for the seesaw region of lighter N.

Therefore, by performing searches for displaced RH neutrinos from the light $B-L$ scalar at the HL-LHC, we can test the type-I seesaw mechanism in a large parameter space, with the help of the precision timing information of CMS/ATLAS or the large MATHUSLA detector on the surface. As this scenario is very similar to that in Ref. [30], where RH neutrinos are instead produced via the $B-L$ gauge boson, a comparison can be made to understand the different phenomenology induced by the nature of the mediator. Indeed, RH neutrinos produced from gauge boson decay are more likely to be distributed in very forward directions compared to those from the scalar. This means that forward detectors like FASER and FACET are more sensitive to the new physics from the exotic gauge boson.

ACKNOWLEDGMENTS

We thank Frank Deppisch and Suchita Kulkarni for useful early discussions. This work is supported by the Natural Science Foundation of Jiangsu Province (Grant No. BK20190067). W. L. is supported by the 2021 Jiangsu Shuangchuang (Mass Innovation and Entrepreneurship) Talent Program (JSSCBS20210213). H. S. is supported by the National Natural Science Foundation of China (Grants No. 12075043 and No. 12147205).

APPENDIX: CALCULATION OF THE TIMING INFORMATION

The time delay of the N decay products can be expressed as $\Delta t \equiv l_N/v_N + l_\ell/c - l_{\rm SM}/c$, where for simplicity we have assumed that the decay products travel at the speed of light c [72] in a straight line, and $l_{N,l,\rm SM}$ are the distances that N, l, and the other SM particles travel. According to Ref. [18], l_ℓ and $l_{\rm SM}$ can be obtained as functions of l_N, $\theta_{N,\ell}$, and $\phi_{N,\ell}$ as

$$
\begin{aligned}
l_\ell^{\parallel} &= l_{T_2}/\sin(\pi-\theta_\ell) - l_N \frac{\sin\theta_N}{\sin(\pi-\theta_\ell)},\\
\vec{l}_\ell &= (l_\ell \sin\theta_\ell \sin\phi_\ell, l_\ell \sin\theta_\ell \cos\phi_\ell, l_\ell \cos\theta_\ell),\\
|l_\ell \sin\theta_\ell| &\approx |l_\ell^{\parallel} \sin\theta_N/\cos(\phi_\ell-\phi_N)|,\\
\vec{l}_N &= (l_N \sin\theta_N \sin\phi_N, l_N \sin\theta_N \cos\phi_N, l_N \cos\theta_N),\\
\vec{l}_{\rm SM} &= \vec{l}_N + \vec{l}_\ell, \qquad l_{\rm SM} = |\vec{l}_{\rm SM}|,
\end{aligned} \tag{A1}
$$

where $\theta_{N,\ell}$ is the angle between the momentum of the N,ℓ to the beam line, $\phi_{N,\ell}$ is the angle between the momentum of the N,ℓ to the x axis, $l_\ell^{\parallel}$ is the length of the parallel component of l_ℓ to the beam axis, and $l_{T_2} = 1.17$ m for the MIP timing detector [79]. Once we get l_N, $\theta_{N,\ell}$, and $\phi_{N,\ell}$ from the Monte Carlo simulation, the time delay can be calculated.

[1] A. Davidson, Phys. Rev. D **20**, 776 (1979).
[2] R. N. Mohapatra and R. Marshak, Phys. Rev. Lett. **44**, 1316 (1980); **44**, 1644(E) (1980).
[3] T. Asaka and M. Shaposhnikov, Phys. Lett. B **620**, 17 (2005).
[4] S. Chatrchyan *et al.* (CMS Collaboration), Phys. Lett. B **717**, 109 (2012).
[5] R. Aaij *et al.* (LHCb Collaboration), Phys. Rev. Lett. **112**, 131802 (2014).
[6] G. Aad *et al.* (ATLAS Collaboration), J. High Energy Phys. 07 (2015) 162.
[7] V. Khachatryan *et al.* (CMS Collaboration), Phys. Lett. B **748**, 144 (2015).
[8] V. Khachatryan *et al.* (CMS Collaboration), J. High Energy Phys. 04 (2016) 169.
[9] E. Cortina Gil *et al.* (NA62 Collaboration), Phys. Lett. B **778**, 137 (2018).
[10] A. Izmaylov and S. Suvorov, Phys. Part. Nucl. **48**, 984 (2017).
[11] A. M. Sirunyan *et al.* (CMS Collaboration), Phys. Rev. Lett. **120**, 221801 (2018).
[12] G. Aad *et al.* (ATLAS Collaboration), J. High Energy Phys. 10 (2019) 265.
[13] R. Aaij *et al.* (LHCb Collaboration), Eur. Phys. J. C **81**, 248 (2021).
[14] R. Aaij *et al.* (LHCb Collaboration), Eur. Phys. J. C **81**, 261 (2021).
[15] A. Tumasyan *et al.* (CMS Collaboration), arXiv: 2201.05578.
[16] A. Atre, T. Han, S. Pascoli, and B. Zhang, J. High Energy Phys. 05 (2009) 030.
[17] F. F. Deppisch, W. Liu, and M. Mitra, J. High Energy Phys. 08 (2018) 181.
[18] J. Liu, Z. Liu, and L.-T. Wang, Phys. Rev. Lett. **122**, 131801 (2019).
[19] J. L. Feng, I. Galon, F. Kling, and S. Trojanowski, Phys. Rev. D **97**, 035001 (2018).
[20] M. Frank, M. de Montigny, P.-P. A. Ouimet, J. Pinfold, A. Shaa, and M. Staelens, Phys. Lett. B **802**, 135204 (2020).
[21] V. V. Gligorov, S. Knapen, M. Papucci, and D. J. Robinson, Phys. Rev. D **97**, 015023 (2018).
[22] S. Cerci *et al.*, J. High Energy Phys. 06 (2022) 110.
[23] J. P. Chou, D. Curtin, and H. J. Lubatti, Phys. Lett. B **767**, 29 (2017).
[24] T. Robens and T. Stefaniak, Eur. Phys. J. C **75**, 104 (2015).
[25] C. Anastasiou, C. Duhr, F. Dulat, E. Furlan, T. Gehrmann, F. Herzog, A. Lazopoulos, and B. Mistlberger, J. High Energy Phys. 09 (2016) 037.
[26] E. Accomando, L. Delle Rose, S. Moretti, E. Olaiya, and C. H. Shepherd-Themistocleous, J. High Energy Phys. 02 (2018) 109.
[27] J. M. Cline and G. Gambini, Phys. Rev. D **105**, 115035 (2022).
[28] F. F. Deppisch, N. Desai, and J. W. F. Valle, Phys. Rev. D **89**, 051302 (2014).
[29] B. Batell, M. Pospelov, and B. Shuve, J. High Energy Phys. 08 (2016) 052.
[30] F. Deppisch, S. Kulkarni, and W. Liu, Phys. Rev. D **100**, 035005 (2019).
[31] B. Bhattacherjee, S. Matsumoto, and R. Sengupta, arXiv: 2111.02437.
[32] A. Das, P. S. B. Dev, and N. Okada, Phys. Lett. B **799**, 135052 (2019).
[33] K. Cheung, K. Wang, and Z. S. Wang, J. High Energy Phys. 09 (2021) 026.
[34] C.-W. Chiang, G. Cottin, A. Das, and S. Mandal, J. High Energy Phys. 12 (2019) 070.
[35] P. Fileviez Pérez and A. D. Plascencia, Phys. Rev. D **102**, 015010 (2020).
[36] S. Amrith, J. M. Butterworth, F. F. Deppisch, W. Liu, A. Varma, and D. Yallup, J. High Energy Phys. 05 (2019) 154.
[37] A. Das, N. Okada, S. Okada, and D. Raut, Phys. Lett. B **797**, 134849 (2019).
[38] W. Liu, S. Kulkarni, and F. F. Deppisch, Phys. Rev. D **105**, 095043 (2022).
[39] C. Han, T. Li, and C.-Y. Yao, Phys. Rev. D **104**, 015036 (2021).
[40] A. Das and N. Okada, Phys. Lett. B **774**, 32 (2017).
[41] A. Pilaftsis, Z. Phys. C **55**, 275 (1992).
[42] M. L. Graesser, Phys. Rev. D **76**, 075006 (2007).
[43] A. Maiezza, M. Nemevšek, and F. Nesti, Phys. Rev. Lett. **115**, 081802 (2015).
[44] M. Nemevšek, F. Nesti, and J. C. Vasquez, J. High Energy Phys. 04 (2017) 114.
[45] J. D. Mason, J. High Energy Phys. 07 (2019) 089.
[46] E. Accomando, L. Delle Rose, S. Moretti, E. Olaiya, and C. H. Shepherd-Themistocleous, J. High Energy Phys. 04 (2017) 081.

[47] Y. Gao, M. Jin, and K. Wang, J. High Energy Phys. 02 (2020) 101.
[48] A. M. Gago, P. Hernández, J. Jones-Pérez, M. Losada, and A. Moreno Briceño, Eur. Phys. J. C **75**, 470 (2015).
[49] J. Jones-Pérez, J. Masias, and J. D. Ruiz-Álvarez, Eur. Phys. J. C **80**, 642 (2020).
[50] T. Robens, in 2022 Snowmass Summer Study (2022), arXiv:2203.08210.
[51] P. S. B. Dev, R. N. Mohapatra, and Y. Zhang, Nucl. Phys. **B923**, 179 (2017).
[52] F. Bergsma *et al.* (CHARM Collaboration), Phys. Lett. **157B**, 458 (1985).
[53] L. A. Anchordoqui, P. B. Denton, H. Goldberg, T. C. Paul, L. H. M. Da Silva, B. J. Vlcek, and T. J. Weiler, Phys. Rev. D **89**, 083513 (2014).
[54] P. S. B. Dev, J.-F. Fortin, S. P. Harris, K. Sinha, and Y. Zhang, J. Cosmol. Astropart. Phys. 01 (2022) 006.
[55] P. Bechtle, S. Heinemeyer, O. Stål, T. Stefaniak, and G. Weiglein, Eur. Phys. J. C **74**, 2711 (2014).
[56] P. Bechtle, O. Brein, S. Heinemeyer, O. Stål, T. Stefaniak, G. Weiglein, and K. E. Williams, Eur. Phys. J. C **74**, 2693 (2014).
[57] G. Cacciapaglia, C. Csaki, G. Marandella, and A. Strumia, Phys. Rev. D **74**, 033011 (2006).
[58] J. Alcaraz *et al.* (ALEPH, DELPHI, L3, OPAL, LEP Electroweak Working Group Collaborations), arXiv:hep-ex/0612034.
[59] E. Bagnaschi *et al.*, Eur. Phys. J. C **79**, 895 (2019).
[60] D. de Florian *et al.* (LHC Higgs Cross Section Working Group), *Handbook of LHC Higgs Cross Sections: 4. Deciphering the Nature of the Higgs Sector* (CERN, Geneva, 2017), Vol. 2, arXiv:1610.07922, https://inspirehep.net/literature/1494411.
[61] C. Degrande, C. Duhr, B. Fuks, D. Grellscheid, O. Mattelaer, and T. Reiter, Comput. Phys. Commun. **183**, 1201 (2012).
[62] A. Alloul, N. D. Christensen, C. Degrande, C. Duhr, and B. Fuks, Comput. Phys. Commun. **185**, 2250 (2014).
[63] N. D. Christensen and C. Duhr, Comput. Phys. Commun. **180**, 1614 (2009).
[64] Feynrulesdatabase, https://feynrules.irmp.ucl.ac.be/wiki/B-L-SM.
[65] J. Alwall, R. Frederix, S. Frixione, V. Hirschi, F. Maltoni, O. Mattelaer, H. S. Shao, T. Stelzer, P. Torrielli, and M. Zaro, J. High Energy Phys. 07 (2014) 079.
[66] T. Sjöstrand, S. Ask, J. R. Christiansen, R. Corke, N. Desai, P. Ilten, S. Mrenna, S. Prestel, C. O. Rasmussen, and P. Z. Skands, Comput. Phys. Commun. **191**, 159 (2015).
[67] M. Cacciari, G. P. Salam, and G. Soyez, Eur. Phys. J. C **72**, 1896 (2012).
[68] J. de Blas *et al.*, J. High Energy Phys. 01 (2020) 139.
[69] P. Draper, J. Kozaczuk, and S. Thomas, J. High Energy Phys. 09 (2020) 174.
[70] E. Izaguirre, G. Krnjaic, and B. Shuve, Phys. Rev. D **93**, 063523 (2016).
[71] D. Krohn, L. Randall, and L.-T. Wang, arXiv:1101.0810.
[72] A. Berlin and F. Kling, Phys. Rev. D **99**, 015021 (2019).
[73] R. Aaij *et al.* (LHCb Collaboration), Eur. Phys. J. C **77**, 224 (2017).
[74] S. Antusch, E. Cazzato, and O. Fischer, Phys. Lett. B **774**, 114 (2017).
[75] A. Ariga *et al.* (FASER Collaboration), Phys. Rev. D **99**, 095011 (2019).
[76] P. D. Bolton, F. F. Deppisch, and P. S. Bhupal Dev, J. High Energy Phys. 03 (2020) 170.
[77] I. Esteban, M. C. Gonzalez-Garcia, M. Maltoni, T. Schwetz, and A. Zhou, J. High Energy Phys. 09 (2020) 178.
[78] N. Aghanim *et al.* (Planck Collaboration), Astron. Astrophys. **641**, A6 (2020); **652**, C4(E) (2021).
[79] CMS Collaboration, Technical Report CERN-LHCC-2017-027/LHCC-P-009, CERN, Geneva (2017), https://cds.cern.ch/record/2296612.